Large-scale soil-structure physical model (1g) - assessment of structure damages

Marwan Al Heib, Fabrice Emeriault, Matthieu Caudron, Luyen Nghiem, Boramy Hor

▶ **To cite this version:**

Marwan Al Heib, Fabrice Emeriault, Matthieu Caudron, Luyen Nghiem, Boramy Hor. Large-scale soil-structure physical model (1g) - assessment of structure damages. International Journal of Physical Modelling in Geotechnics, 2013, 13 (4), pp.138-152. 10.1680/ijpmg.13.00007 . ineris-00961815

HAL Id: ineris-00961815
https://ineris.hal.science/ineris-00961815

Submitted on 20 Mar 2014

HAL is a multi-disciplinary open access archive for the deposit and dissemination of scientific research documents, whether they are published or not. The documents may come from teaching and research institutions in France or abroad, or from public or private research centers.

L'archive ouverte pluridisciplinaire **HAL**, est destinée au dépôt et à la diffusion de documents scientifiques de niveau recherche, publiés ou non, émanant des établissements d'enseignement et de recherche français ou étrangers, des laboratoires publics ou privés.

International Journal of Physical Modelling in Geotechnics
Volume 13 Issue 4

Large-scale soil–structure physical model (1*g*) – assessment of structure damages
Al Heib, Emeriault, Caudron *et al.*

International Journal of Physical Modelling in Geotechnics, 2013, **13**(4), 138–152
http://dx.doi.org/10.1680/ijpmg.13.00007
Paper 1300007
Received 24/06/2013 Accepted 30/09/2013
Keywords: buildings, structure & design/geotechnical engineering/mining & quarrying

ICE Publishing: All rights reserved

ice Institution of Civil Engineers
publishing

Large-scale soil–structure physical model (1*g*) – assessment of structure damages

Marwan Al Heib HDR
Research engineer, Ineris, Nancy, France

Fabrice Emeriault
Professor, Grenoble-INP, Grenoble, France

Matthieu Caudron PhD
Research engineer, EDF, Lyon, France

Luyen Nghiem
PhD student, Ineris, Verneuil-en-Hallate, France

Boramy Hor
PhD student, Ineris, Verneuil-en-Halatte, France

The paper presents a new large small-scale physical model (6 m^3) for studying the damage to structures owing to underground movements: settlement, subsidence and sinkhole. The aim of the research is to study the soil–structure interaction effect of large vertical displacement owing to underground mines. The soil used in the physical model is Fontainebleau sand. The simple masonry structure was built using different materials: polycarbonate, silicone, wood and sugar. The vertical displacement was applied by an electric jack. The physical model is used to reproduce ground surface displacement profiles and the displacement measurement system is based on digital image correlation. Image processing was carried out to analyse the soil and structure displacements. The model allowed comparing the behaviour of soil and structure under different conditions: greenfield and with structure (different positions). Tension cracks appear when the applied subsidence reaches the structure's bearing capacity. The structure damage (cracks) depends on the structure position and the transfer of soil movement to the structure. These results also highlight the importance of the structure position in the development of cracks and damage to the masonry structure. The physical model presents an excellent tool for understanding the behaviour of real buildings and facilities.

Notation

A	cross-section of structure
A_m	maximum subsidence
B	length of structure
D	depth
D_r	relative density
E	elastic modulus of the structure
EA	axial stiffness of the structure
EI	bending stiffness of the structure
E_s	constant elastic modulus of the soil
e	void ratio
e_h	horizontal strain
e_{max}	maximum void ratio
e_{min}	minimum void ratio
H	depth of the cavity
I	inertia of the structure
i	inflexion point
O	open layer
p	tilt
S_{max}	maximum vertical displacement
S_h	horizontal displacement in greenfield conditions
S_v	vertical displacement in greenfield conditions
$S_{(x)}$	vertical displacement following x
W_c	critical width of mine area
α^*	relative axial stiffness
γ	influence angle
θ	maximum strain angle
ρ^*	relative bending stiffness

1. Introduction

Shrinkage and swelling of clays, groundwater lowering, mining activities and collapse of natural cavities could induce the subsidence of ground surface. The occurrence of subsidence of the ground surface can be very damaging to structures and infrastructures and to the safety of people. Damages depend on two main components: the intensity of the subsidence and the structure (position, characteristics, materials, shape, age and design). Recently, several research works have focused on the analysis of the soil–structure interaction phenomena owing to ground movements induced by tunnel and mining excavations (Caudron *et al.*, 2007; Franzius *et al.*, 2004; Giardina *et al.*, 2012; Potts and Addenbrooke, 1997). They used different approaches: in situ monitoring of real structures, small-scale physical model under normal gravity (1***g***) or in centrifuge and numerical simulation.

In the last decade, Ineris has researched the interaction between soil and structures, specifically for underground cavities, using numerical and 1***g*** physical models (Abbass-Fayad, 2004; Caudron *et al.*, 2007; Deck, 2002; Hor *et al.*, 2011). In particular, a large small-scale physical model has been designed to reproduce the phenomena and to assess qualitatively, and to a certain extent quantitatively, the soil–structure interactions and the vulnerability of masonry structures (typically individual houses). The design, use, filling and instrumentation of this physical model are presented in the current paper (in particular the system used to reproduce ground surface displacement profiles and the displacement measurement system based on digital image correlation (DIC)) together with its validation under greenfield conditions (without the structure). Two simplified building models are studied: in the first case the structure is represented by an equivalent slab, in the second the structure is represented by an assembly of blocks with no consideration of mortar in the joints (only frictional resistance is accounted for). Particular attention is paid to the determination of the transfer ratios of movements from the soil to the structure and of the consequences on damage to the structure.

2. Subsidence description and consequences

2.1 The mechanism of subsidence

Mine subsidence corresponds to the collapse of the ground surface over areas where mineral ores have been removed. Subsidence causes ground surface deformation, resulting in a range of problems from deep holes with vertical sides exposing people to danger, to more subtle forms of subsidence characterised by sagging and hogging of the ground surface producing more damage, over larger areas, affecting nearly all man-made structures. Figure 1 presents the theoretical curves of vertical displacement, horizontal displacement, tilt, horizontal strain and curvature in the case of mining. Similar curves can be presented in the case of tunnelling (Al Heib, 2008; Standing and Potts, 2008). The subsidence characteristics depend on the characteristics of the underground cavities (depth, area etc.). The influence angles γ determine the boundaries of the zone of potential impact of subsidence on structures and infrastructures. The maximum damages are generally observed in structures that are located in the zone of maximum horizontal extension strain defined by the angle θ (Figure 1).

2.2 Damage to structures

The impact of subsidence on buildings and infrastructures has become an important and costly environmental issue during mining operations and following mine closures (Edjossan-Sossou *et al.*, 2012; ISRM, 2008). Figure 2 summarises the different components of movements and deformation that can affect the structure due to surface subsidence. Different

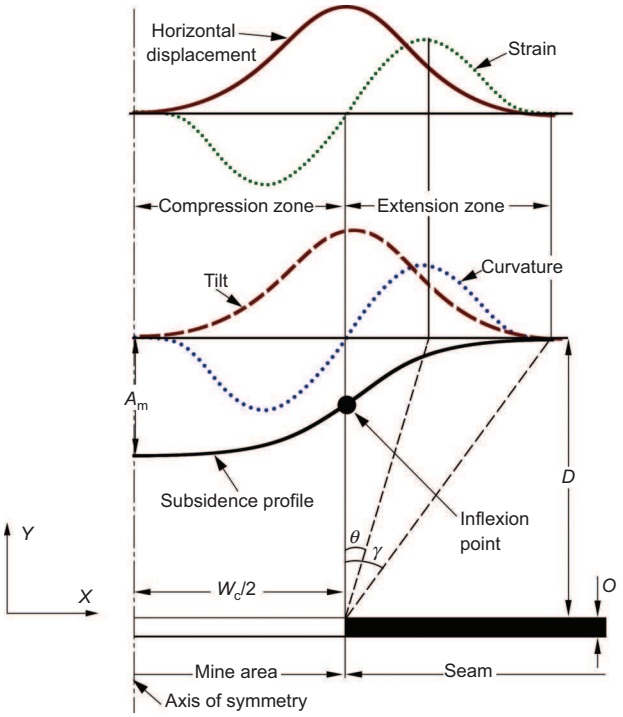

Figure 1. Subsidence parameters (O: open layer, A_m: maximum subsidence, γ and θ: influence angle and maximum strain angle, D: depth, W_c: critical width of mine area)

parameters are defined to qualify the deformation of the structure (Burland and Wroth, 1974). The vertical component of ground movements causes changes in the ground gradient, which can adversely affect, for example, drainage, tall buildings and machinery in factories. Tilting, horizontal strains (extension and compression) and curvature are the causes of the most commonly observed types of damage. Extension is characterised by pulled open joints in masonry. The compressive strains result in the squeezing-in of voids, such as doors and windows, and in the horizontal movements of masonry blocks. The intensity of the horizontal strain is generally used as the key parameter to assess the level of damage (from light to very severe (Burland *et al.*, 1977; NCB, 1975)).

2.3 Mining subsidence and soil–structure interaction

Empirical rules exist for the assessment of building damage caused by such ground movements (Deck, 2002). However, they are limited by the context of their definition. There are very few relationships to determine the damages caused to buildings by ground movements and that explicitly take into account the soil–structure interactions. The existing methods are mainly based on numerical studies (Deck and Harlaka, 2010; Dimmock and Mair, 2008; Potts and Addenbrooke, 1997). The way soil movements affect the structure depends on

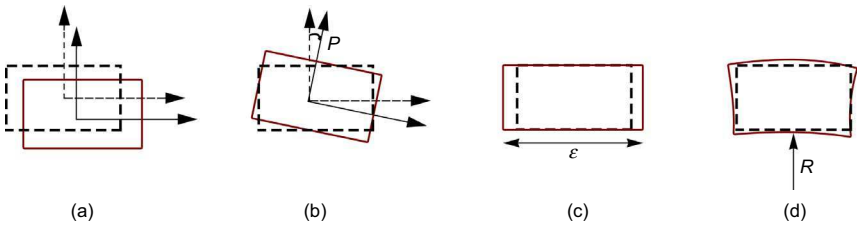

Figure 2. Different types of movement affecting a structure owing to subsidence influence (Deck, 2002): (a) translation; (b) inclination; (c) horizontal strain; (d) curvature

the stiffness of the structure, its age and the type of foundations. Potts and Addenbrooke (1997) showed, using two-dimensional (2D) numerical modelling, that the transfer of soil strains to the structure decreases with the increasing relative bending (ρ^*) and axial (α^*) stiffness (Equations 1 and 2). They are defined by the constant elastic modulus of the soil (E_s) and structure (E) and by the length (B), cross section (A) and inertia of the structure (I) assumed to be equivalent to a beam

$$\rho^* = \frac{16EI}{E_s B^4} \quad (1)$$

$$\alpha^* = \frac{2EA}{E_s B} \quad (2)$$

The soil–structure interaction influences the transfer of strains to buildings and other types of structures. The nature of the subsoil can play a major role in the transfer of underground movement to the structures. Several research projects have focused on analysing the ground–structure interaction phenomena due to several types of soil movements (Abbass-Fayad, 2004; Burd *et al.*, 2000; Deck, 2002; Lee and Bassett, 2007; Nakai *et al.*, 1997; Standing and Potts, 2008; Sung *et al.*, 2006). The present paper will mainly focus on the presentation of soil–structure interaction in the case of mining subsidence using the facility of the physical modelling.

3. Design of a 3D large small-scale physical model for the analysis of the effect of mining subsidence

3.1 State of the art

Investigation of the impact of mining subsidence on infrastructure can be done through the physical modelling. Four types of physical model can be identified following the size of the model: full-scale field tests, small-scale physical field tests, small-scale physical laboratory tests (1***g***) and, finally, small-scale centrifuge tests (Allersma, 1995). The small-scale physical model was adopted in the present study because of its benefits: size reduction, simplification and convenience, possible analysis of situations for which analytical models are too complex, and ultimately possible use of the experimental data as base for the validation of theoretical or numerical models. Nevertheless, it is subject to well-known limitations that are acknowledged in the present case: full compliance with scaling laws is often impossible; the performance capabilities of test facility influence the modelling, design and manufacturing; measurement and testing costs affect modelling and designs (Muir Wood, 2004). Very few small-scale physical models have been used to study the effects of ground movements caused by mining operations or by the collapse of old mines. The first physical model was presented by Knothe in 1950 in which sand was used to describe the subsidence.

Recently, Dyne (1998) conceived a trap door type model in order to represent the occurrence of sinkholes in an old coalmine in Pennsylvania. The model has a trap door with four different widths and a single layer of sand as overburden. Castro *et al.* (2007) and Trueman *et al.* (2008) dedicated their study to the block caving exploitation method. Aydan *et al.* (2010) studied the effect of an earthquake on the stability of an old coalmine in Japan. They showed that depending on the geometry the failure may occur in the pillars or at the mine ceiling. Ren *et al.* (2010) carried out several tests with a 1***g*** small-scale physical model to determine the parameters of the subsidence. Bachmann (2006) performed a three-dimensional (3D) physical modelling of large-scale gravitational rock mass movements. He used an analogue materials and an original experimental gravity loading device, allowing tests to be carried out in compliance with the different scaling laws. He *et al.* (2009) developed a large-scale physical model simulating geological horizontal strata. They studied the deformation and the failure processes of roadways subjected to a plane loading scheme. Tests have been performed in the context of the European Union research project Quaker to study the influence of several buildings, considering different geometries,

weights and foundation systems, on the path followed by a fault activated by the Kocaeli earthquake (Bransby *et al.*, 2008a, 2008b). None of the tests considered the potential damages caused by subsidence on the buildings.

3.2 Design of the Ineris small-scale physical model

To design the large small-scale model the following postulates must be considered: the design hypotheses of the physical model depend on the purpose of the tests and on the constructive characteristics of the prototype. Obviously, some of these design hypotheses are a consequence of the scaling laws. The physical model must be a true scalar representation of the prototype. The length scale defining the model dimension is considered a fundamental quantity within the model's design. The boundary conditions must enable the model to move and deform in a manner similar to the prototype.

According to the postulates, the physical model is designed to be used in a 1***g*** environment (earth gravity). The objective of the physical model is to simulate the surface ground movements owing to mining and underground cavities. The large small-scale model must be able to hold a soil block of 3 × 2 × 1 m. The main aim of the Ineris physical model is to measure the surface deformation and building damage caused by an underlying trough (Figure 3). The movements at ground surface are achieved by vertical downwards movements of electric jacks placed at the bottom of the model. The control of the velocity and the magnitude of the vertical movement are both realised using computer and commercial software. The cross-section of the actuator is limited to 250 × 250 mm, corresponding to up to 12·5 × 12·5 m at prototype scale. The apparatus is indeed limited to localised phenomena: small sinkhole or collapse/subsidence of limited extent. The initial design of the model allows the installation of a collection of several jacks in order to reproduce various shapes and extents of collapse/subsidence. The purpose is to be able to model, for example, a chosen area from a subsidence trough observed in a mining basin and then to study the effects of this particular trough on the buildings and the protection potential of several mitigation techniques.

3.3 Measurement technique

Measurement of surface displacements is achieved by means of stereo digital imagery. The DIC technique was used to determine the displacements and deformations. DIC allows monitoring the whole surface of the ground and more especially where ground movements occur. The commercial software VIC3D from Limess GmbH was chosen, after analysing different commercial software, owing to its effectiveness in computing sand grain movements showing very low contrast (Son *et al.*, 2012). VIC3D provides full-field, 3D measurements of shape, displacement and strain. The usual performances of VIC3D used on solid and continuous specimens range for strains from 50 microstrain to 2000% strain and above, for specimen sizes ranging from <1 mm to >10 m. The first application proposed by Hor *et al.* (2011) to granular materials such as sand have shown that the global precision is equivalent to 0·05 pixel). Son *et al.* (2012) used a three-dimensional digital image correlation (3D DIC) analysis to investigate the displacements on the surface of a dense sand specimen during a triaxial compression test. The relative position of the two cameras (see Figure 3) is very precisely known as well as the distance to the zone of maximum movements. In these conditions, the global precision of 3D displacements of the soil and structure surfaces is 0·02 mm in vertical and in plane horizontal directions and 0·10 mm in the horizontal out of plane direction (Figure 3).

The two high-resolution digital cameras, 4 megapixels each, have a maximum frequency of 8 images/s at full resolution, with the possibility of reaching 30 images/s with a 1 megapixel resolution. They must be calibrated before the start of a test by

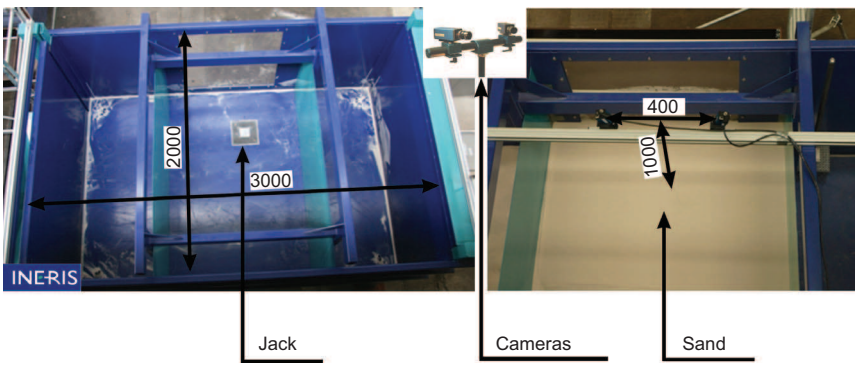

Figure 3. Large small-scale physical model for modelling surface subsidence and damage to structures. All dimensions are in mm

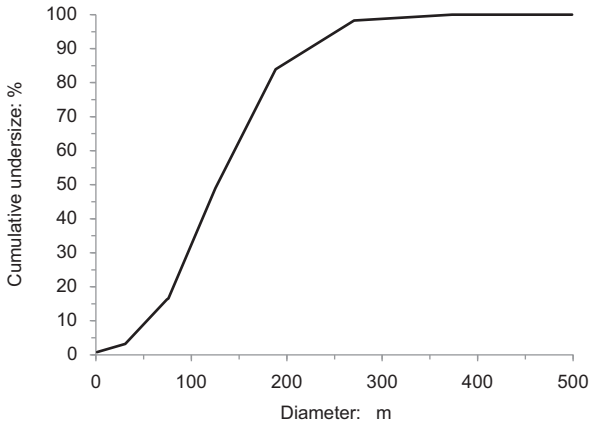

Figure 4. Grading curve of Fontainebleau NE34 sand

means of a test pattern. A good calibration allows obtaining very accurate measurements with an error of 1/100 of a pixel in good conditions: this corresponds to 10 μm when 1 pixel is equal to 1 mm. The precision of the measurement is close to 5/100 pixel. In the tests presented later in this paper, this ratio is close to 2 pixels per millimetre. However, because the sand used in the experiments cannot be considered a true continuous media (being constituted of small particles), the corresponding maximal error has been estimated to be close to 0·10 pixel (corresponding to 0·0 mm), which is still a good performance (Correlated Solutions, 2010; White *et al.*, 2003). The application of the DIC method requires the physical determination of the horizontal distance between the two cameras (400 mm), and the determination of the angle between the two-camera axis through the use of a calibration target (the calibration target is imaged simultaneously in both cameras, and the synchronised target images are used to fully calibrate the system in one step).

The main disadvantage of this method of monitoring is the huge volume of data created by a single test. With a volume of 8 MB per capture (two images of 4 MB each) and considering the maximum frequency of capture, nearly 2 GB of raw data need to be stored each minute. For a full test and with the exploitation files for the digital correlation process, this corresponds to a total required memory volume of between 30 and 40 GB. The localisation of the cracks (opening joints) is determined using a correlation quality indicator provided by VIC3D for each correlation analysis. A statistical confidence region, in pixels, based on the analysis of covariance matrix of the correlation equation is calculated. If the corresponding variable (denoted sigma) exceeds a given threshold, the data are removed from the analysis. It gives a direct feedback (a qualitative scale) on the data quality but also on the occurrence of a crack: when a crack appears, a strong discontinuity of displacements is generally observed resulting in a sudden change in the value of sigma. Each crack is then affected to a certain class of damage based on the value of sigma.

4. Validation of the physical model under greenfield conditions

4.1 The analogue soil

A model soil was used for the validation of the ability of the physical model to reproduce phenomena observed at large scale. Even though this soil is cohesionless, in future it will be possible to use cohesive material (with the appropriate installation methods). The considered model soil is Fontainebleau sand (essentially silica with silicon dioxide (SiO_2) > 98%), well known to researchers in physical geotechnical modelling (Garnier, 2002). This sand is very smooth and for our purposes category NE 34 sand was chosen. The considered grade of Fontainebleau sand (D_{50} = 200 μm) has on the one side less negative effects, due to scale ratio of the physical model, on the transfer of movement from soil to structure than another type of sand, but on the other side, allows the use of DIC with a satisfying accuracy of the displacements determination. The grading curve and mechanical characteristics of NE 34 sand are presented in Figure 4 and Table 1. The results were obtained from laboratory tests (shear and triaxial tests). The density and mechanical characterisations vary according to the degree of compaction. The density of the Fontainebleau sand is determined as a function of the value of the void ratio (e). The concept of the relative density (D_r) was adopted. The relative density of the granular soils such as sand can be determined by $D_r = (e_{max} - e)/(e_{max} - e_{min}) \times 100$ with e_{min} and e_{max}: minimum and maximum void ratios determined according to standard test procedures. Loose sand is considered when the relative density ranges between 0 and 40%, medium sand corresponds to values

State	Unit weight: kN/m^3	D_r: %	Young modulus E: MPa	Peak friction angle: °	Residual friction angle: °
Dense	16·00	79	5 to 20	35 to 42	27 to 31
Medium	15·42	44	—	30 to 36	24 to 33
Loose	15·00	31	—	29 to 33	33 to 28

Table 1. Main physical and mechanical characteristics of Fontainebleau NE 34 sand

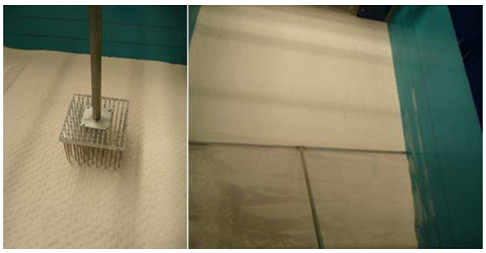

Figure 5. (a) Procedure of the sand compaction and (b) the procedure to obtain a horizontal surface

between 40 and 80% and dense sand when D_r is larger than 80%. With the consideration installation procedure, the average value of D_r for the Fontainebleau sand used in the physical model is equal to 44–49%, therefore very close to medium sand. These tests have been performed at very low stress considering the thickness of the soil layer used in the model and the stress applied on the ground surface. The range of values given in Table 1 for the friction angles therefore include the effect of repeatability tests and that of the accuracy of the conventional test apparatus at low stress. Furthermore, in that range, soil exhibits a non-linear shear resistance, values of the friction angle depend on the way the results of tests are interpreted.

4.2 Test procedure

The sand is manually placed in the tank by layers of 15 cm thickness. Each layer is compacted by a compacting tool equipped with 15 cm long needles in order to ensure the required level of density, repeatable for each test (Figure 5(a)). This is repeated until the total height of the soil layer is

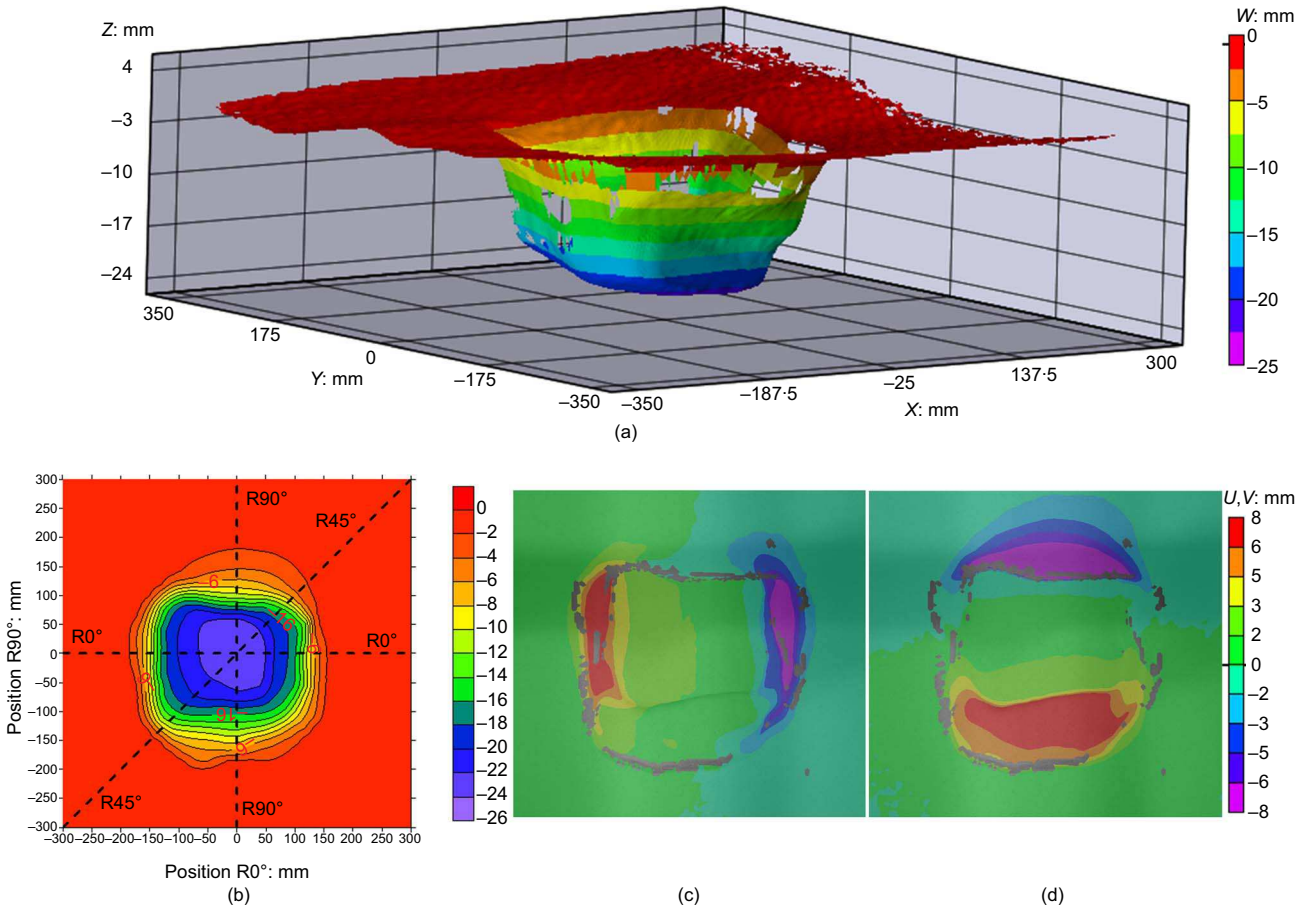

Figure 6. (a) 3D view of the settlement trough, (b) 2D view of the iso-contours of settlements, (c)(d) 2D view of the horizontal displacements in *X* direction and *Y* direction. Displacement fields have been obtained with a 300 m thick sand layer and a 30 mm vertical displacement of the jack – displacements are given in mm

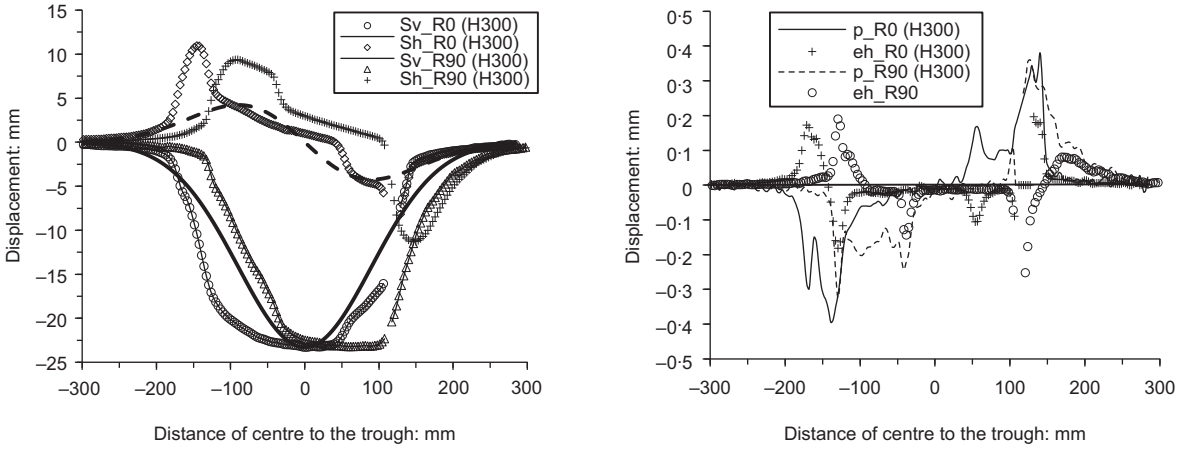

Figure 7. Vertical (S_v) and horizontal (S_h) displacements in greenfield conditions and corresponding theoretical curves (peck = subsidence and lake (horizontal displacement); tilt (p) and horizontal strain (e_h) (H300: corresponds to the thickness of the sand layer (mm) and R90 is the vertical profile)

reached, in this case, 30 cm. Finally, a 130 cm wide rule is used to obtain the correct horizontal level on the whole ground surface (Figure 5(b)). Dynamic penetrometer tests (Panda) were used to determine the density of the sand (GTR, NF P11-300), and the results (D_r = 44 to 49%) indicate that the sand is close to medium state in depth and to loose state on the surface.

A snapshot is then taken by both cameras to ensure that the ground surface is flat enough with a tolerance of less than 5 mm over the whole 3 m × 2 m and respectively gives a maximum slope of 0·16% and 0·25% of the length and width apparatus. The building model is placed delicately on the ground surface for different positions. The acquisition by the two cameras is then started with a frequency of 0·5 Hz (one image every 2 s). At the same time, the program controlling the displacement of the jack is launched. The jack is moved downwards with a constant velocity of 0·15 mm/s for a total displacement of 30 mm. At the end of the test, the displacements of the ground surface (and in the sequel of the structure) are computed by the DIC program. The treatment of images allows the determination of vertical and horizontal displacements and strains (Figure 6). Different profiles can be drawn to analyse the soil and structure behaviour. At the end of the experiment, in order to determine the total displacement of the soil under the structure, the structure is carefully removed and an addition image of the soil is taken.

4.3 Analysis of the tests under greenfield conditions

To validate the design of the large-scale physical model and the test procedure and post-treatment, a vertical movement of the jack is applied at the bottom of the sand layer with a constant velocity of 0·15 mm/s. The total vertical movement of the jack (displacement) is 3 mm corresponding to 1·2 m in reality considering the adopted scale factor (1/40). Four identical tests were performed in order to ensure a good level of repeatability. As shown in Figures 6 and 7, the greenfield subsidence trough can be considered to be symmetric. The characteristics of the subsidence (vertical displacement, horizontal displacement, maximum tilt and horizontal strain) were determined along different horizontal directions. Three profiles have been considered for the exploitation of the results. In the tests involving soil–structure interaction, these profiles correspond to the lines going from the centre of the building to the centre of the subsidence trough. The extension of the subsidence trough is limited to 300 mm, corresponding to an influence angle of 45°. The maximum vertical displacement (surface subsidence) is equal to 85% of the vertical displacement applied at the bottom of the soil layer. The average global characteristics are summarised in Table 2. The difference from

Characteristics of subsidence trough	Value used in the physical model
Maximal vertical displacement S_{vmax}: mm	24
Maximal horizontal displacement S_{hmax}: mm	9·8
Maximal tilt: m/m and %	0·4, i.e. 40%
Maximum horizontal strain ε_h: m/m and %	0·2, i.e. 20%

Table 2. Characteristics of the surface subsidence

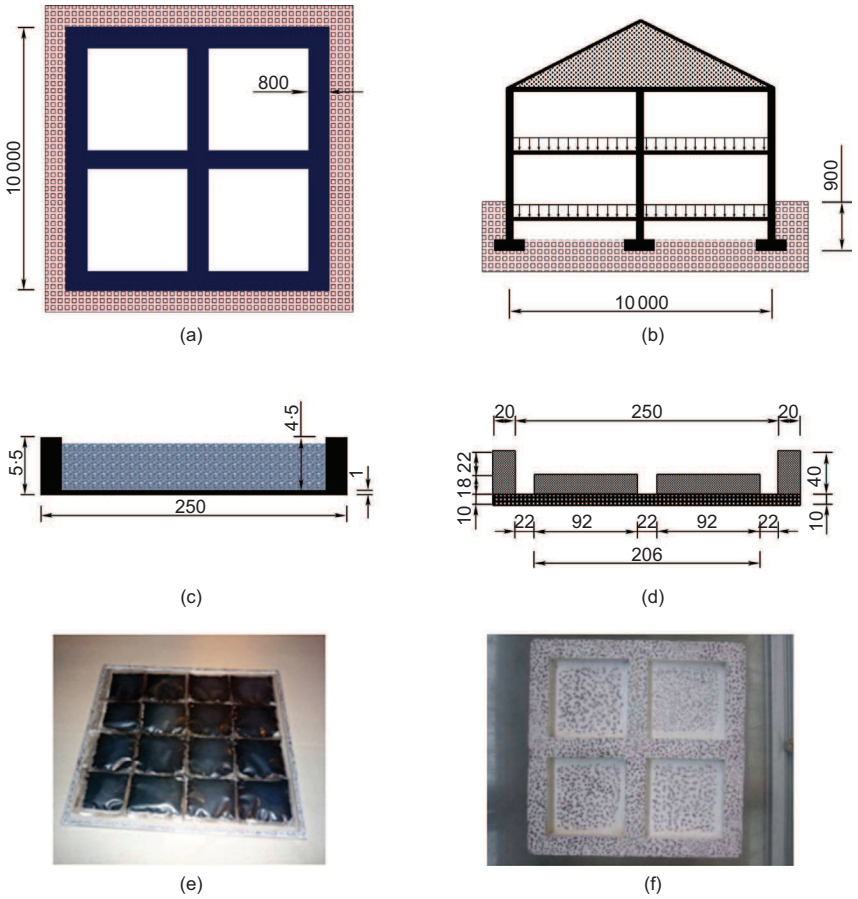

Figure 8. Description of the prototype structure ((a) plane view, (b) cross-section), of small-scale model in polycarbonate ((c) cross-section, (d) view with the dead load applied by bags of lead balls) and in silicone ((e) cross-section, (f) plane view). All the dimensions are in mm

Parameter	Scaling factor	Prototype	Ideal model	Polycarbonate	Silicone
Width: m	40	10	0·25	0·25	0·25
Length: m	40	10	0·25	0·25	0·25
Height: mm	40	250	6·25	4·5	40
Young modulus E: MPa	40	30 000	750	2200–2500	5
Weight: kN	40^3	1000	$15{\cdot}6 \times 10^{-3}$	$15{\cdot}6 \times 10^{-3}$	$21{\cdot}5 \times 10^{-3}$
EA: MN	40^3	$7{\cdot}5 \times 10^4$	1·17	0·75	0·036
EI: N.m^2	40^5	$3{\cdot}9 \times 10^4$	3·81	2·86	3·3
ρ*	1	$3{\cdot}9 \times 10^{-3}$	$3{\cdot}9 \times 10^{-3}$	$3{\cdot}9 \times 10^{-3}$	$4{\cdot}5 \times 10^{-3}$
α*	1	2	2	2	0·096

Table 3. Simplification procedure of the 3D building to an equivalent small-scale slab

one test to another is less than 15% and can be considered acceptable in this experimental context. The maximum horizontal displacement is equal to 9·8 mm corresponding to 41%, very close to theoretical and empirical relations given by Peck (1969) for the vertical displacement (Equation 3, with $S_{(x)}$ vertical displacement, S_{max}: maximum vertical displacement, i: inflexion point) and Lake for the horizontal displacement (Equation 4, with H the depth of the cavity) (Lake *et al.*, 1992, Figure 7). With the two empirical equations (3 and 4), one can calculate the displacements for different distances (x) from the centre of the trough. The ability of the physical model is to reproduce in situ observations in the case of green field conditions.

3. $$Sv_{(x)} = S_{max} e^{-x^2/2i^2}$$

4. $$Sh_{(x)} = Sv_{(x)} \frac{x}{H}$$

Table 2 summarises the maximum parameters of the subsidence. The values of tilt and horizontal strain are very high if a structure is directly impacted by the corresponding settlement trough; one can expect it to be damaged.

5. Assessment of soil–structure interaction with simplified structure models

5.1 The structure

In order to study the effects of the soil–structure interactions during the occurrence of a subsidence trough, an individual house is used for testing. The reference geometry for the building is based on the analysis of an existing database of individual buildings damaged by mining subsidence in the east of France (Deck, 2002). A typical 10 m × 10 m two-floor house constituted of masonry walls (Young modulus: 6000 MPa and Poisson ratio: ν = 0·3), reinforced concrete slabs (Young modulus: 30 000 MPa, Poisson ratio ν = 0·2) and shallow foundations is considered. This realistic prototype scale model has been simplified to define the small-scale model.

The first physical model of structure corresponds to a simple equivalent slab. The 25 × 25 cm surface of the slab is relevant with the prototype (10 m × 10 m) with a scale ratio equal to 1/40. It is determined by the nature of the material characterised by Young's modulus and the thickness of the slab e. These two elements are combined to obtain a bending stiffness EI and an axial stiffness EA of the slab equivalent to those of the 3D structure, taking into account the scaling laws (Garnier *et al.*, 2007). Theoretically, the correct thickness should be 50 cm at prototype scale according to the approach of Potts and Addenbrooke (1997). The adopted thickness is equal to 25 cm and both bending and axial stiffness are approximately halved.

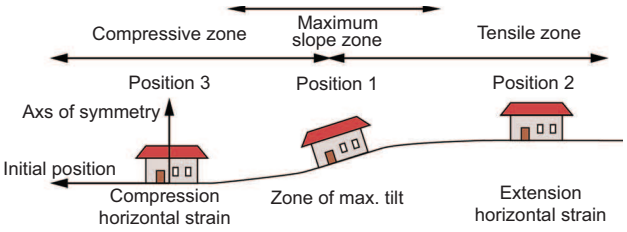

Figure 9. Building position for the parametric study

Two materials are used to represent the slab in the small-scale physical model: polycarbonate and silicon. The polycarbonate slab corresponds to a simple sheet. The silicon slab's geometry is more complex with the height of the edges equal to 40 mm and the height of the inside equal to 18 mm (Figure 8). The thickness of the polycarbonate slab is reduced as well as it weight (it is

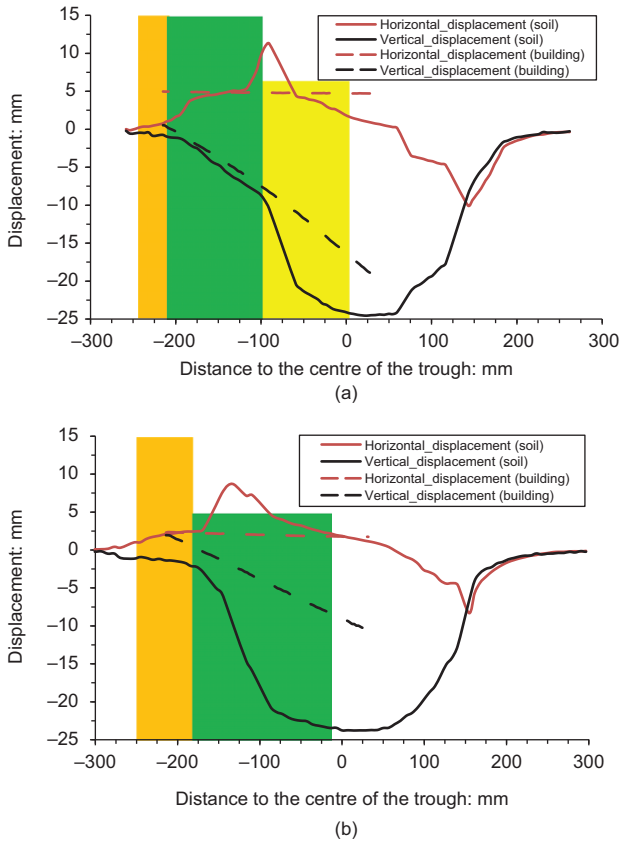

Figure 10. Behaviour of the ground for two different positions of the building: (a) position 1; (b) position 2). Colours show the different cases of soil–structure contact: structure lying on the ground (green), contact lost between structure and ground (orange: rise of the building due to rigid body rotation, yellow: loss of support)

Case	Horizontal strain: %	Bending – radius of curvature: m	Tilt: %
Greenfield (position 1)	−5	—	21·6
SSI (position 1)	−0·21	—	6·4
Greenfield (position 2)	−10·5	−1·67	21·6
SSI (position 2)	−0·24	−9·42	11·1

Table 4. Comparison between the parameters of the main deformation modes determined under greenfield conditions and using the building model (soil structure interaction – SSI)

therefore loaded with small bags of lead balls in order to apply on the ground surface the correct equivalent weight of the structure). The silicone slab has a high thickness and a small Young's modulus. Owing to the geometric and mechanical characteristics, the silicone slab has a smaller axial stiffness (−95%) and a greater bending stiffness (+17%) than the polycarbonate slab. Table 3 summarises the main characteristics of the two small-scale models of the slab (polycarbonate and silicon). The adopted scale factor herein is (1/40). This table highlights the difference between the ideal model parameters (corresponding to the scaled values of the prototype characteristics) and the values used in the two simplified models of the structure.

The polycarbonate slab is placed directly on the ground, and the contact between the slab and the soil only mobilises the friction angle of the interface. This limits the interaction between the soil and the structure. However, it is very easy to reproduce this procedure over several tests.

5.2 Results obtained with the polycarbonate structure

Three positions of the structures with respect to the centre of the subsidence trough were studied with the equivalent slab model (Figure 9). They are actually defined with respect to the main component of the subsidence trough and related loading mechanisms. Position 1 corresponds to the maximum slope, position 2 mainly to an extension and position 3 corresponds to the compression zone of the trough's centre. Four tests were performed for each position of the building, as under the greenfield condition. Results are then presented from two points of view. First, the displacements measured at ground surface are compared with those obtained in greenfield conditions in order to identify the effect of the building on the ground behaviour. Second, the strains of the building model and the transfer ratio are determined.

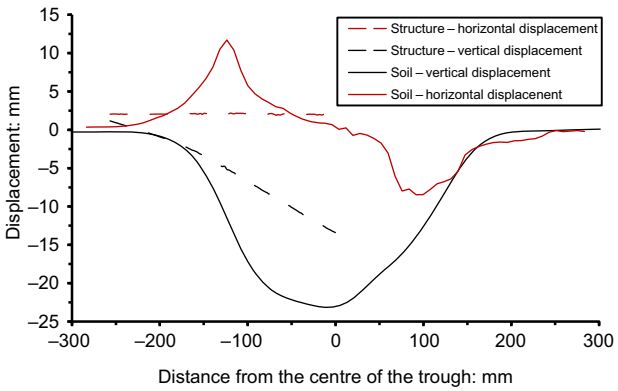

Figure 11. Subsidence trough due to a 30 mm vertical displacement of the jack with silicone slab in position 2

5.2.1 Effect of the structure on the ground subsidence

The building causes some important differences in the soil displacement at ground surface. The trough, symmetric under greenfield conditions, shows clearly a dissymmetric shape, except for the case of position 3 (Figure 9), centred in the subsidence trough, where the displacements remain symmetric. Two examples of ground displacement curves are shown in Figure 10, corresponding to the profiles plotted for the position 1 (Figure 10(a)) and position 2 (Figure 10(b)) of the soil and the building (in these figures, the horizontal axis goes along an axis of symmetry of the structure and intersects the vertical axis of symmetry of the jack and therefore of the reference greenfield settlement trough). The final soil displacements were obtained after removing carefully the structure. It appears that the soil movements are reduced due to the effect of the soil–structure interaction. Different areas may be distinguished, depending on the relative displacement of the ground to the building model. In the central part of the trough, the ground falls off the building owing to greater displacement, whereas on the other side of the building, its rotation causes another loss of contact between soil and model.

5.2.2 Effect of the subsidence trough on the structure's behaviour

The 3D movements and deformations of the building can be accurately determined by means of the DIC system and further compared to the soil displacements and strains under greenfield conditions. In addition, the transfer ratio between the soil and

	Soil		Structure	
Parameter	Greenfield	Soil–structure interaction	Polycarbonate	Silicone
Vertical soil displacement, max: mm	24	25	11	20·1
Horizontal soil displacement, max: mm	9·8	11·1	1·93	3·84
Max soil tilt: %	40	30	6·4	5·13
Horizontal soil compression strain, max: %	20	—	0·08	0·61

Table 5. Subsidence and structure characteristics for two configurations: greenfield conditions and structure in position 2

the structure deformations responsible for the damage to the structure are determined. The horizontal extension/compression, bending and tilt are summarised in Table 4. It appears that the horizontal strains of the slab are very small compared to the corresponding soil deformation in greenfield conditions. The polycarbonate slab mainly rotates and the slope is equal to approximately half of the slope of the soil. Two possible explanations for this observation are the large relative stiffness of the building and the fact that the building is just lying on the ground surface (no embedment depth). The soil–structure interaction is thus clearly identifiable: the behaviour of the soil is substantially modified due to the presence of the building, and consequently the strains measured in the structure are different from those calculated using the ground displacement in greenfield conditions.

5.3 Effect of the flexibility and embedment depth of the structure: silicone slab

Figure 11 presents the profiles of vertical and horizontal displacement of both the soil surface and the silicone slab structure for position 2. Table 5 presents the main parameters of the subsidence phenomenon compared with the greenfield situation. One can observe the reduction of the amplitude of vertical and horizontal displacements and maximum tilt as for the polycarbonate slab. Even though the effect of the structure is clearly apparent, the reduction of the parameters is not as significant.

One can observe that the vertical displacement of the structure is smaller than the vertical soil displacement (Table 5), indicating a loss of contact between soil and structure at the corner of the slab close to the centre of the subsidence trough. The comparison between the two slabs confirms the influence of the structure's stiffness. All the displacements and tilt are greater for the polycarbonate slab than for the silicone slab. The horizontal compression strain is eight times more sensitive for the silicon slab than for the polycarbonate slab. Table 6 also shows that the ratio between soil and structure displacement varies as a function of the material characteristics: because of its flexibility, the silicon slab follows the soil movement, whereas the polycarbonate slab behaves as a cantilever beam. Within the range of loads applied to the slab in both cases, it is noteworthy that polycarbonate and silicon still behave as elastic materials, even if the deformations considered at the prototype scale would cause severe damage to the structure. In order to reproduce damage and collapse of the structure, it is necessary to consider other models of structures and materials. This result confirms the importance of the stiffness, in particular the axial stiffness of the slab. In addition, the silicone slab is partly embedded in the ground, whereas the polycarbonate slab is just resting on the soil surface owing to its limited thickness. The potential damage to the silicone slab is greater than that to the polycarbonate slab (if the strength characteristics of these two materials were compatible with compression or extension plasticity and failure). In both cases the corresponding strains are very substantial for a real structure.

Parameter	Prototype blocks	Ideal model	Sugar	Wood
L · l · h: mm	500 × 250 × 200	12·5 × 6·25 × 5	27 × 18 × 12	7 × 7 × 14
Young modulus *E*: GPa	10 000		Not determined	16 000–19 000
Unit weight: kN/m^3	19·0	19·0	15·90	10·30
Friction angle between blocs φ: °	20–35	20–35	30	30 ± 9

Table 6. Characteristics of equivalent masonry blocks

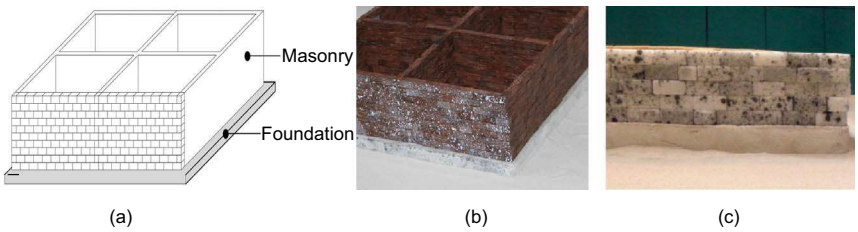

Figure 12. Small-scale model of masonry structure (wood or sugar blocks) and foundation (silicon): (a) model; (b) wood; (c) sugar

6. Assessment of soil–structure interaction with realistic structure models

6.1 Masonry structure

The structure model has been improved by adding the principal walls of the masonry structure (Figure 12): the material used to reproduce the masonry in the small-scale model is wood or sugar pieces. The sugar pieces used come from the commercial markets. The wood type used herein is Azobe, corresponding to very dense wood associated with high compression strength. There is no mortar between blocks, the friction angle being large enough to allow the transfer of displacements and stresses between blocks. The main advantage of masonry blocks without mortar is the early initiation of damage to the structure with limited soil displacements and deformations. The main inconvenience is that the model will not reproduce the behaviour of a typical masonry structure after the initiation of the first crack and in particular the possible localisation of damage in a limited number of cracks. The mechanical parameters of sugar and wood blocks have not been determined for this study. The construction of the structure model is realised manually. It uses the silicone slab as a foundation system.

Table 6 summarises the characteristics of the masonry materials (prototype, sugar and wood). The actual scale factor (1/40) is not respected. The difference between wood and sugar concerns the block dimensions and the corresponding Young's modulus. The sugar blocks are two to three times larger than the wood pieces. The wood pieces are cut to represent more closely real masonry blocks. The blocks are rigid and damage will be essentially observed at the joints (normal opening or tangent relative displacement).

6.2 Results for the masonry structure in position 2

For the purpose of the test (mainly feasibility), the masonry structure was located at the ground surface (with an embedment depth of the silicone slab foundation) in the maximum tilt zone corresponding to position 2 (Figure 9). The embedment improves the soil–structure interaction and the transfer of soil movement to the surface structure; it also corresponds to the reality, even with good quality soil and limited applied loads. The maximum of the applied vertical displacement is 30 mm (1·2 m in the real scale). The result of tests on the masonry structure using the sugar and the wood pieces are presented in Figures 13 and 14, respectively.

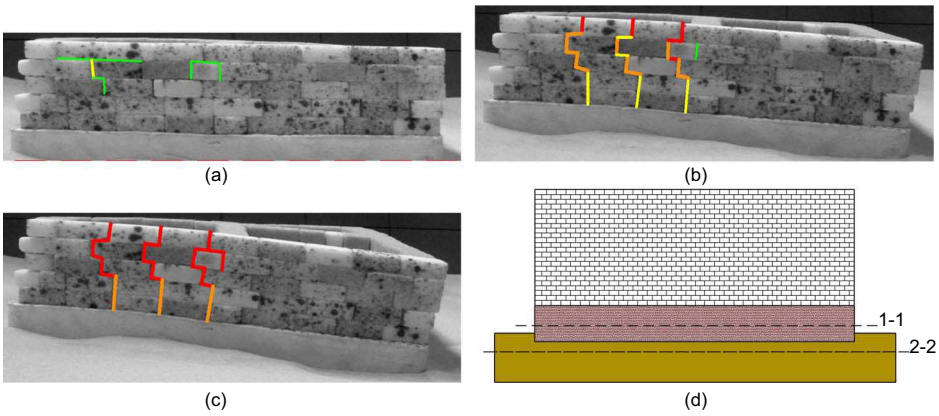

Figure 13. Progress of the damage to the masonry structure (sugar pieces) owing to increasing vertical displacement of the soil: (a) 3·3 mm, (b) 13·2 mm and (c) 30 mm (Figure 13(d): position of the profiles 1-1 and 2-2 for the displacement measurements respectively on the foundation and at the ground surface). Scale of damage: green – negligible damage, orange-yellow – intermediate damage, red – severe damage

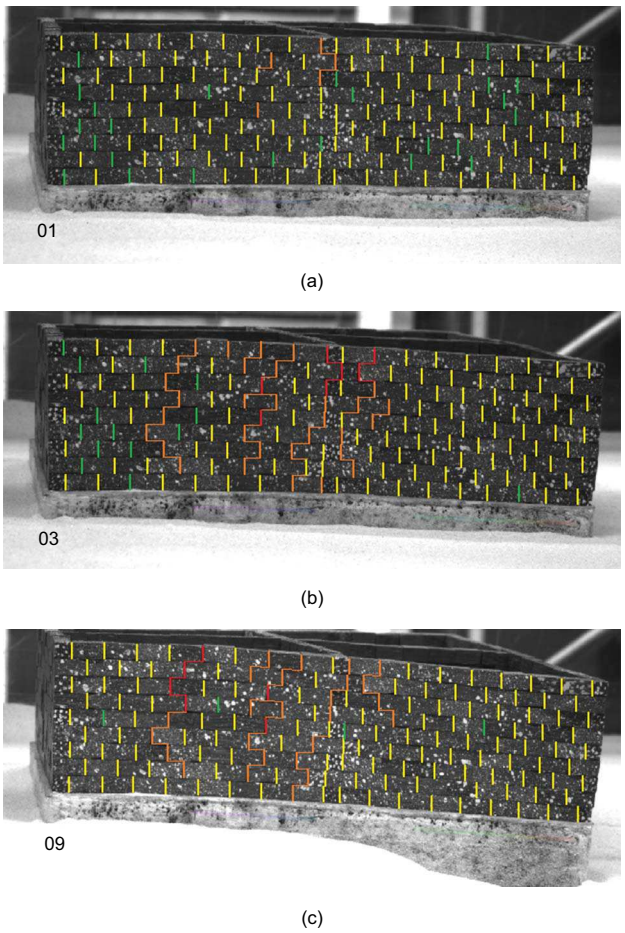

Figure 14. Progress of the damage to the masonry structure (wood pieces) owing to increasing vertical displacement of the soil owing to increasing vertical displacement of the soil: (a) 3·3 mm, (b) 13·2 mm and (c) 30 mm. Scale of damage: green – negligible damage, orange-yellow – intermediate damage, red – severe damage

Table 7 presents the tilt of the silicon slab (measured on the foundation, profile 1-1 defined in Figure 13) and of the soil close to the foundation (profile 2-2) for two identical tests performed with wood blocks. The silicone foundation is flexible and the relative axial stiffness (approximately 10^{-2}) is very small. It allows a good transfer of horizontal strain following the Potts and Addenbrooke (1997) approach. The transfer ratio of the tilt varies between 69% and 97%. The ratio is very high compared to the case using a polycarbonate foundation. Severe damage to the masonry structure is observed owing to the tilt of the foundation and the associated deflection ratio (0·6%), which is also a measure of the building's curvature.

	Wood masonry structure	
	Test 1	Test 2
Tilt of the silicone foundation: %	4·8	6·23
Tilt of the soil: %	7	6·38
Transfer ratio: %	69	97·80

Table 7. Tilt and transfer ratio of the wood masonry structure

The DIC technique makes it possible to determine the development and localisation of the principal joint opening (fissures or cracks) by measuring the normal distance between two blocks initially in contact. Three main classes are considered: green for negligible damage for very small cracks with a width less than 0·1 mm, yellow for intermediate damage, the width of cracks is less than 5 mm, and the red class corresponds to a severe damage, the width of cracks is greater than 5 mm (Figure 13). The first opened joint between sugar blocks is observed for a vertical surface displacement of 3 mm and only one or two blocks are concerned (Figure 13). The opening of the joint is smaller than 0·025 mm (1 mm at the prototype scale). The number of opened joints increases with the vertical displacement of the jack. The width of the opening joints increases up to 0·375 mm. At the end of the test, it can be assumed that the vertical cracks develop across the structure from the bottom to the top. The localisation of vertical cracks corresponds to the limit of the contact between the soil and the structure. The foundation induces the opening of the joints between blocks.

The use of the wood pieces (that approximately respect the scale factor) confirms the masonry structure behaviour and the development of opening joints (Figure 14). The localisation of opening joints in the wood structure corresponds to those obtained in the sugar structure. The opening of the joints, in the case of the wood pieces, is much smaller than the sugar pieces. The identification of a privileged direction of opening cracks is more delicate than in the case of sugar pieces. The pieces of the wood are smaller, so the localisation of cracks is different and concerns larger zones compared to the sugar structure. This result can help to understand the role of the dimensions of masonry structure blocks in subsidence zones.

7. Conclusions and outlook

This paper presents a new apparatus (medium-sized physical modelling facility) to model ground movements caused by the collapse of underground cavities. A description of the model (design, material, image treatment etc.) has been given in the paper. The Fontainebleau sand, digital cameras and VIC3D software and electric jack were used to model and determine underground movement. A simple model of structure using different materials (polycarbonate, silicone, wood and sugar), was designed. It represents at the prototype scale a typical

individual house and is used for two main purposes: to observe the evolution of the ground movements (with or without the building model) and to analyse the behaviour of the building itself and, thus, to shed some light on the importance of the soil–structure interaction. It can be concluded from this study that the soil–structure phenomenon must not be neglected and that it depends greatly on the relative position of the building in the subsidence trough.

The apparatus enables the effect at the ground surface of the failure of the typical case of a mine located 20 m below ground level with a 10×10 m^2 cross-sectional area of extraction to be reproduced with a scale factor of 1/40. Several models have been developed to mimic the behaviour of a typical 10×10 m two-floor individual house made of masonry. This large small-scale model appears to be a very useful tool for studying the soil–interaction phenomena.

Concerning the structure behaviour, a stiff structure behaves like a cantilever beam and ground displacements transferred to the structure are smaller than for a flexible structure. A first approach has been proposed for the analysis of the damage to a masonry structure by means of sugar and wood blocks. This approach shows that the damages to the structure were located clearly in the zone of maximum tilt. The open cracks in the structure model made of sugar blocks are more localised than the ones in the model made of wood blocks perhaps owing to the differing dimensions of the blocks and the friction angle between blocks. With either type of block, it is possible to determine during the subsidence the location and the size of damages in masonry structures.

Despite the encouraging results presented in this paper, one must not forget the limitations and simplifications of the considered cases compared to real-life situations (mainly the fact that the scaling laws are not totally fulfilled in this 1***g*** small-scale physical model). This research should be pursued to improve the physical modelling of the soil and masonry structures. Further research should also propose reference results for the validation of theoretical or numerical methods to determine the type and amount of damage to structures.

REFERENCES

Abbass-Fayad A (2004) *Modélisation Numérique et Analytique de la Montée de Cloche des Carrières à Faible Profondeur. Etude de l'Interaction Sol–structure due aux Mouvements du Terrain Induits par des Fontis*. PhD thesis, Institut National Polytechnique de Lorraine, France (in French).

Allersma N (1995) Simulation of subsidence in soil layers in a geotechnical centrifuge. In *Land Subsidence: Proceedings of the Fifth International Symposium on Land Subsidence* (Barends FBJ, Brouwer FJJ and Schröder FH (eds)). IAHS Press, Wallingford, UK, publication no. 234, p. 117.

Al Heib M (2008) State of the art of the prediction methods of short and long-term ground movements (subsidence and sinkhole) for the mines in France. In *Coal Geology Research Progress* (Michel T and Fourner H (eds)). Nova Science, Hauppauge, NY, USA, pp. 53–76.

Aydan A, Ohta O and Genis M (2010) Response and stability of underground structures in rock mass during earthquakes. *Rock Mechanics and Rock Engineering* **43(6)**: 857–875.

Bachmann D (2006) *Modélisation Physique Tridimensionnelle des Mouvements Gravitaires de Grande Ampleur en Milieu Rocheux*. PhD thesis, Université de Nice-Sophia Antipolis, Nice, France (in French).

Bransby M, Davies M and Nahas A (2008a) Centrifuge modelling of normal fault-foundation interaction. *Bulletin of Earthquake Engineering* **6(4)**: 585–605.

Bransby M, Davies M, Nahas A and Nagaoka S (2008b) Centrifuge modelling of reverse fault-foundation interaction. *Bulletin of Earthquake Engineering* **6(4)**: 607–628.

Burd HJ, Houlby G, Augarde C and Liu G (2000) Modelling tunneling-induced settlement of masonry building. *Proceedings of the Institution of Civil Engineers – Geotechnical Engineering* **143(1)**: 17–29.

Burland JB and Wroth CP (1974) Settlement of buildings and associated damage. *Proceedings of Conference on Settlement of Structures*. Pentech Press, London, UK, pp. 611–654.

Burland, JB, Broms BB and Mello VFB (1977) Behaviour of foundations and structures. *Proceedings of 9th International Conference on Soil Mechanics and Foundation Engineering, Japan*, vol. 2, pp. 495–546.

Castro R, Trueman R and Halim A (2007) A study of isolated draw zones in block caving mines by means of a large 3D physical model. *International Journal of Rock Mechanics and Mineral Science* **44(6)**: 860–870.

Caudron M, Emeriault F and Al Heib M (2007) Contribution of the experimental and numerical modelling to the understanding of the soil–structure interaction during the event of a sinkhole. *Proceedings of the 14th European Conference on Soil Mechanics and Geotechnical Engineering, ECSMGE 2007*, *Madrid*, *Spain*.

Correlated Solutions (2010) *VIC3D Testing Guide*. Correlated Solutions, Columbia, SC, USA. See http://www.correlatedsolutions.com/index.php/vic-3d/ (accessed 06/11/2013).

Deck O (2002) *Etude des Consequences des Affaissements Miniers sur le Bati: Proposition pour une Methodologie d'Evaluation de la Vulnerabilite du Bati*. Thesis, Institut National Polytechnique de Lorraine, France (in French).

Deck O and Harlaka A (2010) Numerical study of the soil–structure interaction within mining subsidence areas. *Computers and Geotechnics* **33(6)**: 802–816.

Dimmock PS and Mair RJ (2008) Effect of building stiffness on tunnelling-induced ground movement. *Tunnelling and Underground Space Technology* **23(4)**: 438–450.

Dyne L (1998) *The Prediction and Occurrence of Chimney Subsidence in South Western Pennsylvania*. MSc thesis, Virginia Polytechnic Institute and State University, Blacksburg, VA, USA. See http://scholar.lib.vt.edu/theses/available/etd-02698-141841/unrestricted/etd.PDF.

Edjossan-Sossou A, Al Heib M, Deck O and Verdel Th (2012) Gestion durable des risques liés à des mouvements de terrains d'origine minière: choix de stratégies – application au cas de Moyeuvre-Grande (57). In *Comptes Rendus des Journées Nationales de Géotechnique et de Géologie de l'Ingénieur, JNGG 2012, Bordeaux.* Comité Français de Mécanique des Sols et de Géotechnique, Rueil-Malmaison, France, pp. 675–682 (in French).

Franzius JN, Potts, DM, Addenbrooke TI and Burland JB (2004) The influence of building weight on tunnelling-induced ground and building deformation. *Soils and Foundations* **44(1)**: 25–38.

Garnier J (2002) Properties of soil samples used in centrifuge models. In *Physical Modelling in Geotechnics: Proceedings of the International Conference, St John's, Canada* (Phillips R, Guo PJ and Popescu R (eds)). Balkema, Rotterdam, the Netherlands, pp. 5–19.

Garnier J, Gaudin C, Springman SM *et al.* (2007). Catalogue of scaling laws and similitude questions in geotechnical centrifuge modelling. *International Journal of Physical Modelling in Geotechnics* **7(3)**: 1–23.

Giardina G, Marini A, Hendriks MA, Rots JA and Rizzardini F (2012) Experimental analysis of a masonry façade subject to tunnelling-induced settlement. *Engineering Structures* **45**: 421–434.

He MC, Gong WL, Li DJ and Zhai HM (2009) Physical modelling of failure process of the excavation in horizontal strata based on IR thermography. *Mining Science and Technology* **19(6)**: 689–698.

Hor B, Caudron M and Al Heib M (2011) Experimental analysis of the impact of ground movements on surface structure. *Proceedings of Pan-America Conference on Soil Mechanics and Geotechnical Engineering, Toronto, Canada*.

ISRM (International Society of Rock Mechanics) (2008) *Mine Closure and Post-mining Management: International State of the Art*. ISRM, Lisbon, Portugal. See http://www.ineris.fr/centredoc/CDi__mineclosure_29_11_08-ang.pdf (accessed 06/11/2013).

Lake LM, Rankin WJ and Hawley J (1992) *Prediction and Effects of Ground Movements Caused by Tunnelling in Soft Ground Beneath Urban Areas*. Construction Industry Research and Information Association (Ciria), London, UK, CP/5, Ciria Funders Report.

Lee YJ and Bassett RH (2007) Influence zones for 2D pile–soil–tunnelling interaction based on model test and numerical analysis. *Tunnelling and Underground Space Technology* **22(3)**: 325–342.

Muir Wood D (2004) *Geotechnical Modelling*. Spon Press, Oxfordshire, UK.

Nakai T, Xu L and Yamazaki H (1997) 3D and 2D model tests and numerical analyses of settlements and earth pressures due to tunnel excavation. *Soils and Foundations* **37(3)**: 31–42.

NCB (National Coal Board) (1975) *Subsidence Engineer's Handbook*. NCB, London, UK.

Peck RB (1969) State of art: deep excavation and tunneling in soft ground. *Proceedings of the 7th International Conference of Soil Mechanics, Mexico*.

Potts D and Addenbrooke T (1997) A structure's influence on tunnelling induced ground movements. *Proceedings of the Institution of Civil Engineers – Geotechnical Engineering* **125(2)**: 109–125.

Ren W, Guo C, Peng Z and Wang Y (2010) Model experimental research on deformation and subsidence characteristics of ground and wall rock due to mining under thick overlying terrain. *International Journal of Rock Mechanics and Mining Science* **47(4)**: 614–624.

Son A, Medina-Cetina Z and Rechenmacher A (2012) Local deformation analysis of a sand specimen using 3D digital image correlation for the calibration of a simple elasto-plastic model. In *GeoCongress 2012 – State of the Art and Practice in Geotechnical Engineering* (Hryciw RD, Athanasopoulos-Zekkos A and Yesiller N (eds)). ASCE, Reston, VA, USA, Geotechnical Special Publication no. 225, pp. 2292–2301.

Standing JR and Potts DM (2008) Contributions to *Géotechnique* 1948–2008. *Géotechnique* **58(5)**: 391–398.

Sung E, Shahin H, Nakai T, Hinokio M and Makoto Y (2006) Ground behaviour due to tunnel excavation with existing foundation. *Soils and Foundations* **46(2)**: 189–207.

Trueman R, Castro R and Halim A (2008) Study of multiple draw-zone interaction in block caving mines y means of a large 3D physical model. *International Journal of Rock Mechanics and Mining Sciences* **45(7)**: 1044–1051.

White DJ, Take WA and Bolton MD (2003) Measuring soil deformation in geotechnical models using digital images and PIV analysis. *Proceedings of the 10th International Conference on Computer Methods and Advances in Geomechanics, Tucson, Arizona, USA*, pp. 997–1002.

WHAT DO YOU THINK?

To discuss this paper, please email up to 500 words to the editor at journals@ice.org.uk. Your contribution will be forwarded to the author(s) for a reply and, if considered appropriate by the editorial panel, will be published as discussion in a future issue of the journal.

International Journal of Physical Modelling in Geotechnics relies entirely on contributions sent in by civil engineering professionals, academics and students. Papers should be 2000–5000 words long (briefing papers should be 1000–2000 words long), with adequate illustrations and references. You can submit your paper online via www.icevirtuallibrary.com/content/journals, where you will also find detailed author guidelines.